SCIENTIFIC REPORTS

OPEN

SUBJECT AREAS:
CONJUGATED POLYMERS
NANOPARTICLES
MICRORESONATORS
COLLOIDS

Received
28 April 2014

Accepted
15 July 2014

Published
31 July 2014

Correspondence and requests for materials should be addressed to A.L. (axel.lorke@uni-due.de) or Y.Y. (yamamoto@ims.tsukuba.ac.jp)

* These authors contributed equally to this work.

Self-assembled conjugated polymer spheres as fluorescent microresonators

Kenichi Tabata[1]*, Daniel Braam[2]*, Soh Kushida[1], Liang Tong[1], Junpei Kuwabara[1], Takaki Kanbara[1], Andreas Beckel[2], Axel Lorke[2] & Yohei Yamamoto[1]

[1]Division of Materials Science and Tsukuba Research Center for Interdisciplinary Materials Science (TIMS), Faculty of Pure and Applied Sciences, University of Tsukuba, 1-1-1 Tennodai, Tsukuba, Ibaraki 305-8573, Japan, [2]Faculty of Physics and Center for Nanointegration Duisburg-Essen (CENIDE), University of Duisburg-Essen, Lotharstraβe 1, Duisburg, D-47048, Germany.

Confinement of light inside an active medium cavity can amplify emission. Whispering gallery mode (WGM) is one of mechanisms that amplifies light effectively by confining it inside high-refractive-index microstructures, where light propagates along the circumference of a sphere via total internal reflection. Here we show that isolated single microspheres of 2–10 μm diameter, formed from self-assembly of π-conjugated alternating copolymers, display WGM photoemission induced by laser pumping. The wavelengths of the emission peaks depend sensitively on the sphere size, position of the excitation spot and refractive index of each polymer. The *Q*-factor increases with increasing sphere diameter and displays a linear correlation with the reciprocal radius, indicating that the small curvature increases the efficacy of the total internal reflection. WGM photoemission from π-conjugated polymer microspheres is unprecedented and may be of high technological impact since the microspheres fulfill the role of fluorophores, high-refractive-index media and resonators simultaneously, in addition to their simple fabrication process.

π-Conjugated polymers play key roles in organic optoelectronics devices such as solar cells[1,2], electroluminescent (EL) devices[3] and light-emitting field-effect transistors[4,5], where the polymers act as charge transporting, light-absorbing and/or emitting layers. One of challenging issues in organic and polymer EL devices is to realize enhanced emission and lasing[3,6–8]. In general, this requires confinement of light in a cavity, *e.g.* a Fabry-Pérot type resonator[7,9]. Confinement is also possible using high-refractive-index microstructures, where total internal reflection takes place inside the microstructures[7,9,10]. Constructive interference occurs when the effective optical path is an integer multiple of the wavelength, which leads to sharp and periodic emission lines. The light generated under such a mechanism is called whispering gallery mode (WGM) photoemission. So far, WGM photoemission and lasing have been reported on inorganic microdisks and spheres[9–14]. In addition, several organic microstructures exhibit WGM emission such as polymer disks, rings, spheres and fibers[15–19], as well as droplets of liquids and liquid crystals[20,21], most of which consist of a dielectric medium doped with a fluorescent dye.

In this paper, we report that self-assembled π-conjugated polymer microspheres, without complicated fabrication processes and dye doping, exhibit WGM photoemission, as confirmed by means of the microphotoluminescence (μ-PL) technique[22]. The major challenge when studying WGM is the fabrication of well-defined, geometrically isotropic spheres. Because π-conjugated polymers tend to crystallize anisotropically due to their rigid and planer backbone[3], limited examples have so far been reported on spheres from π-conjugated polymers[23–25]. In this context, we recently reported that several π-conjugated alternating copolymers such as compounds **1**–**3** (Figs. 1a–1c) self-assemble to form well-defined spheres quantitatively with diameters (*d*) of sub- to several-micrometers[26,27]. These polymers consist of two different arylene groups in the repeating unit. Owing to the highly twisted main chain, these polymers have a weak tendency to crystallize, thus allowing the formation of structurally isotropic spheres. According to X-ray diffraction and spectroscopic studies, polymers in the spheres are in an amorphous state[27]. In the present research, we further find that π-conjugated copolymer **4** (Fig. 1d)[28,29], consisting of azobenzene and aniline repeating units, also forms well-defined microspheres quantitatively.

Results

Preparation of π-conjugated polymer microspheres. The microspheres were prepared by slow precipitation from a solution of the π-conjugated polymers (Fig. S1). Typically, a 5-mL vial containing 2 mL of $CHCl_3$ solution of the polymers (concentration: 1 mg mL^{-1}) was placed in a 50-mL vial containing 5 mL of MeOH. The outer vial

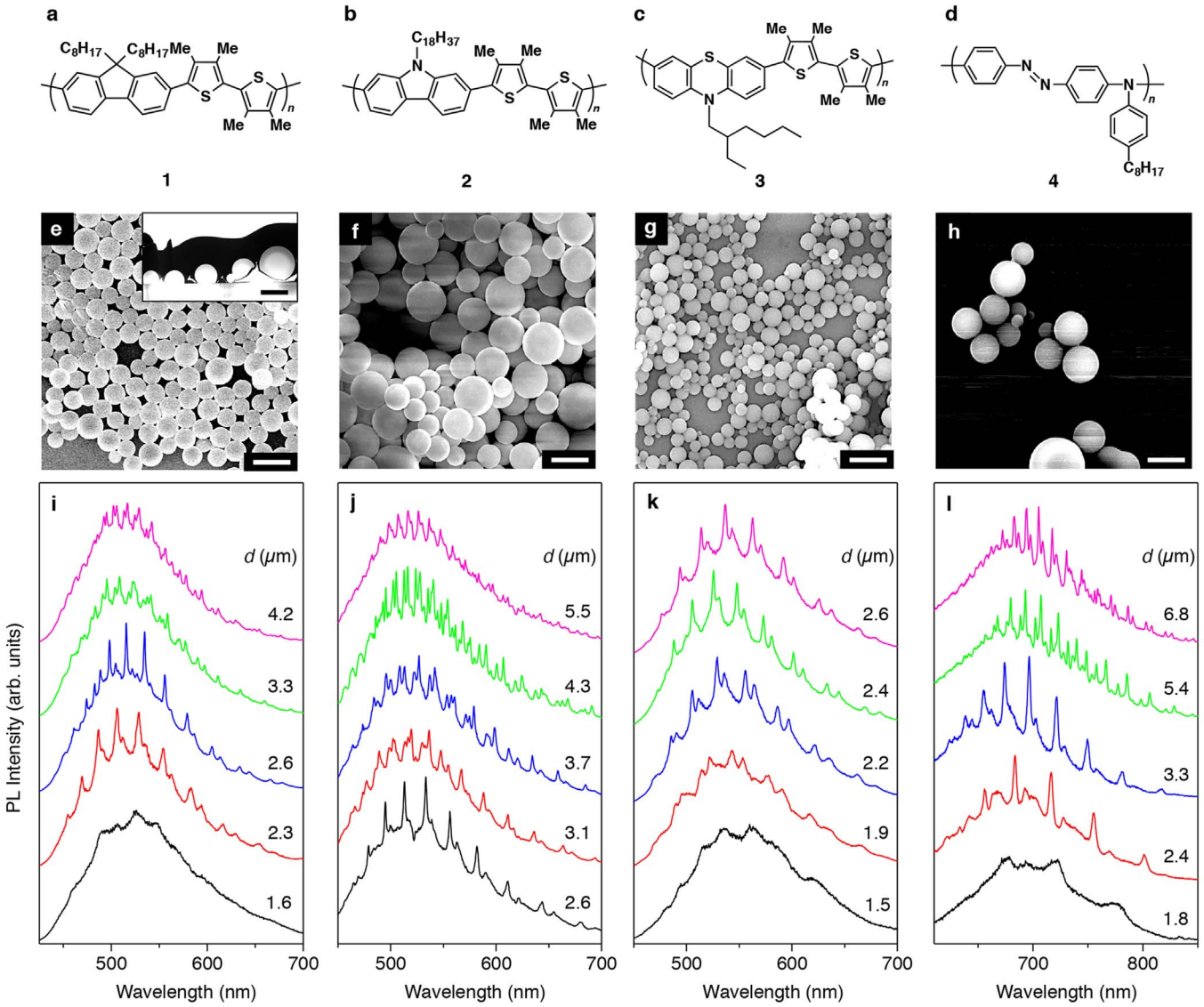

Figure 1 | WGM photoemission from π-conjugated polymer microspheres. (a–d) Molecular structures of π-conjugated alternating copolymers **1**–**4**. (e–h) SEM micrographs of the self-assembled spheres formed from polymers **1**–**4**. Scale bars: 5 μm. Inset in (e) shows a XSTEM image of the self-assembled spheres of **1**. Scale bar: 3 μm. (i–l) PL spectra of a single sphere formed from polymers **1**–**4**. The PL intensity was normalized by the intensity of the broad PL peak commonly observed in all spectra. The numerical values in (i)–(l) indicate the diameters of the single sphere as observed by optical microscopy (with an error margin of $\pm$0.2 μm).

was capped and kept at 25°C in a thermostat bath. The MeOH vapor gradually diffused into the solution of the polymers. The reduced solubility led to precipitation, resulting in a suspension of the polymer microspheres after 3 days of aging. Figures 1e–1g show scanning electron microscopy (SEM) images of the self-assembled microspheres of polymers **1**–**4**, respectively. The sizes of the spheres were typically 1–10 μm in diameter, which depended on the precipitation rate, *e.g.*, the solubility of the polymers, the initial concentration and the setting temperature[26]. Cross-section scanning transmission electron microscopy (XSTEM) shows that the spheres are homogeneously filled with the composed polymer (Fig. 1e, inset).

Photoluminescence from a single sphere. A suspension of the polymer microspheres was spin-cast onto a 200-nm-thick SiO_2-covered Si substrate and air-dried to immobilize the spheres on the substrate (Fig. S2). Figure 1i shows the μ-PL spectra of a single sphere of **1** under laser excitation at the edge of the spheres (excitation wavelength, λ_{ex} = 405 nm, experimental set-up, see Fig. S3). The photoluminescence (PL) spectrum of a sphere with d of 1.6 μm displays a broad photoemission, with a maximum of approximately 525 nm. Also, weak intensity modulation can be observed. By contrast, the PL spectrum of the sphere with d of 2.3 μm exhibits about a dozen periodic peaks superimposed upon the broad photoemission. As the sphere diameter is further increased, the spacing and the width of the sharp emission lines decrease. Microspheres of polymers **2**–**4** show similar PL behavior, where sharp peaks appear when d of the spheres is larger than 2 μm. The larger spheres exhibit much more closely spaced emission lines (Figs. 1j–1l).

It is obvious that these characteristic peaks are not caused by an intrinsic property of the polymer main chain because the position and spacing change depending on the diameter of the spheres. In fact, such sharp and periodic photoemissions were not observed by μ-PL measurements of thin films of these polymers prepared from their $CHCl_3$ solutions (Fig. S4), and also not observed in PL of thin films of the spheres.[25] The observed peaks are attributed to WGM photoemission resulting from the interference of the confined light inside the microspheres. π-Conjugated polymers possess refractive indices

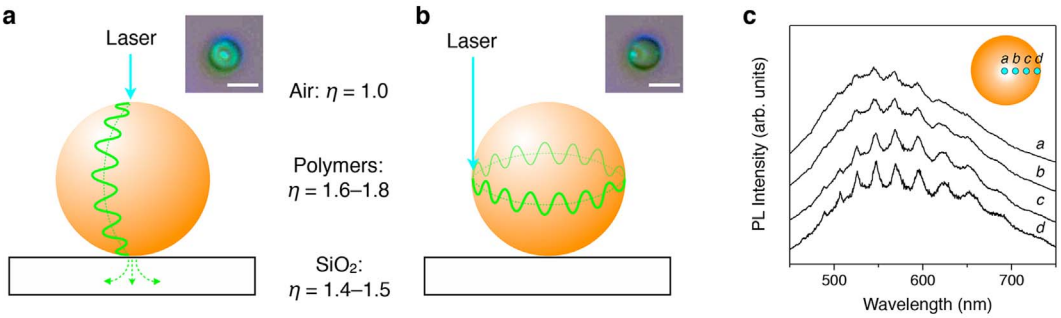

Figure 2 | Excitation position dependence on WGM photoemission. (a, b) Schematic representation of the laser excitation at the center (a) and edge (b) of a microsphere. Blue arrows and green wavy lines indicate the excitation laser and the emission propagating inside the sphere, respectively. Insets show photographs of the top view of the microspheres upon irradiation to the laser at the center (a) and edge (b) of the spheres of **2**. Scale bars: 2 μm. (c) PL spectra of a microsphere ($d \sim 3.5$ μm) consisting of polymer **1** with different position of the laser excitation spots. Inset shows a schematic representation of the top view of a single sphere, showing the excitation spots *a* (center) to *d* (edge).

($\eta_{polymer}$) of 1.6–1.8 at their PL wavelength region (Fig. 3, inset), which is much higher than that of air ($\eta_{air} \sim 1.0$). Accordingly, the generated emission toward the in-plane direction of the spherical surface travels around inside the sphere along the maximum circumference. When the phase of the emitted light coincides in one-circle propagation, resonant emission appears, accompanying the sharp and periodic lines. Spheres with *d* smaller than 2 μm do not show such clear WGM photoemission, possibly because the large curv-

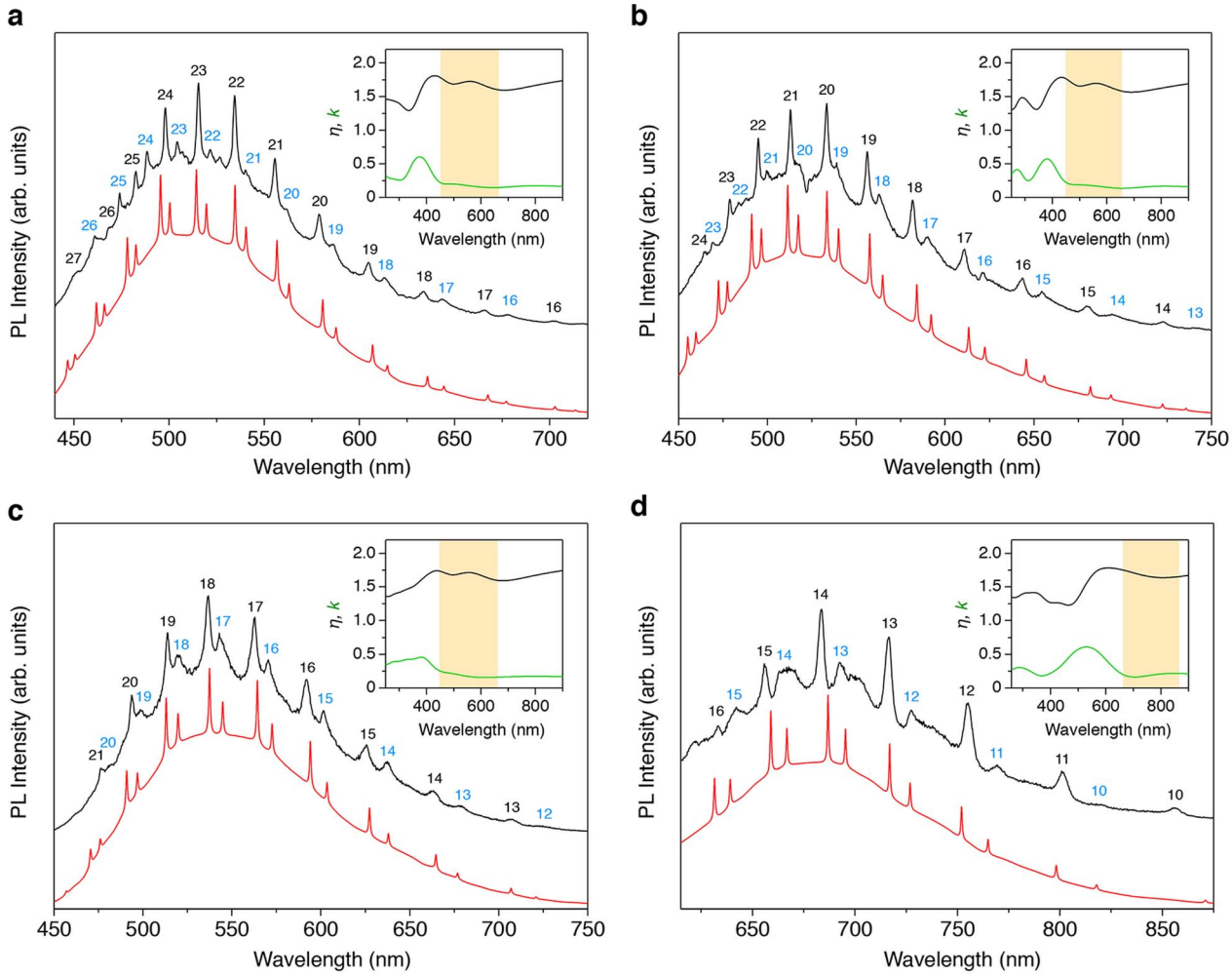

Figure 3 | Identification of the WGM modes. PL spectra (black) of single microspheres consisting of polymers **1** (a), **2** (b), **3** (c) and **4** (d) with diameters of 2.6 μm (a–c) and 2.4 μm (d). The red curves indicate the simulated spectra, obtained from a combination of equations S1 and S2, superimposed on the broad background emission. The peak width in the simulated curves was chosen to roughly reproduce the experimental lines. The black and blue numbers indicate WGM indices for TE and TM mode emissions, respectively. Insets show real (η, black) and imaginary (k, green) parts of refractive indices of the corresponding polymers with respect to the wavelength. The orange-colored regions indicate the range of the photoemission wavelength. For better fitting simulations, averaged η values of 1.70, 1.67, and 1.67 were used for polymers **1**, **2** and **3**, respectively, while the η values at each wavelength were used for polymer **4**.

ature of the spherical surface inhibits the total internal reflection at the boundary of the sphere.

The WGM photoemission is further evidenced from the dependence on the position of the excitation spot. When the top of the sphere is excited, the generated emission inside the sphere always passes through the contact point with the substrate (Fig. 2a). Because the refractive index of SiO_2 (η_{SiO2}: 1.4–1.5) is larger than η_{air} and close to $\eta_{polymer}$, the propagating light inside the sphere leaks out at this point, so that the WGM is effectively damped. On the other hand, when the edge of the sphere is excited (Fig. 2b), the emitted light can propagate around the circumference of the sphere without passing through the contact point with the substrate. In fact, the emission lines upon excitation of the top of the sphere was relatively small in comparison with the background emission, but, as the excitation point is close to the edge of the sphere, the emission lines becomes much clearer (Fig. 2c).

Characterization of WGM photoemission. Resonant emission occurs when the optical path length coincides with an integral multiple of the emission wavelength. As the first approximation, the WGM photoemission follows the equation

$$\eta\pi d = n\lambda \quad (1)$$

where η is the refractive index of the medium, n is an integer and λ is the wavelength of the emission[30]. Figure 3 shows the PL spectra of a single sphere of **1**–**4** with d of 2.4–2.6 μm. Obviously, the observed WGM photoemissions are much more complicated than those expected from equation (1). We conducted simulations using equations S1 and S2 in the Supplementary Information with transverse electric (TE) and magnetic (TM) mode emissions, respectively, as much higher-order approximations[31]. Because the η values of π-conjugated polymers vary with their wavelength, the η values obtained by spectroscopic ellipsometry measurements were used (Fig. 3, insets). The simulated peak positions agree well with those in the observed spectra, where 10–27 reflections of the TE and TM waves are identified in the spheres. The refined d values of the spheres, evaluated from the best-fitted simulations, are 2.71, 2.53, 2.32 and 2.34 μm for spheres of **1**–**4**, respectively. These values from the spectroscopy data are more accurate than those obtained by optical microscopy.

The WGM emissions for spheres with different diameters were also indexed (Figs. S5a–S5d), and the refined d values are listed in Table S1. As the diameter increases, the indices increase owing to the increase of the optical path length. Spheres of **1**–**3** with identical diameters display similar index values because the wavelength regions of the photoemission are similar for these polymers (Figs. S4a–S4c). By comparison, the index values are relatively small for spheres of **4** (Fig. 3d) owing to the longer wavelength emission (Fig. S4d) in comparison with those for spheres of **1**–**3**.

Table S1 also lists the maximum Q-factors of the WGM photoemission of each sphere. Plots of the Q-factors versus the diameters of the spheres show a clear correlation (Fig. 4). The Q-factors are only around 100 for spheres with d of 2 μm; the Q-factors increase as d increase and reach ~600 for the sphere with d of ~10 μm. The plots of Q-factors versus reciprocal radius r^{-1} ($=2d^{-1}$; curvature of the spheres) show an approximately linear correlation (Fig. 4, inset). We attribute the observed correlation to the fact that the large curvature inhibits the total internal reflection of the emission in the sphere.

Coating microspheres with high-refractive-index materials. We conducted durability tests of the WGM emission against laser irradiation. Figure S6a shows the PL spectral change upon taking up to 100 consecutive spectra, each with 0.25 s laser irradiation. The WGM PL becomes weaker as the laser irradiation time increases, possibly because of photoinduced damage of the polymers. However, we found that the damping of the WGM emission can effectively be suppressed by coating the spheres with a thin layer of TiO_x. For the coated samples, the WGM emission is not visibly decaying even after taking 100th spectra (Figs. S6b–S6d).

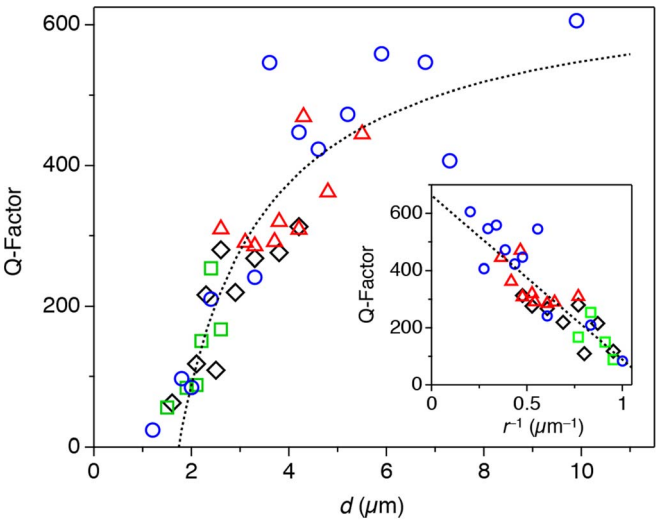

Figure 4 | Relationship between Q-factors and diameters. Plots of the maximum Q-factors of the WGM emission peaks from each sphere versus diameters of the spheres. The rectangular (black), triangular (red), square (green), and circular (blue) symbols represent spheres formed from polymers **1**–**4**, respectively. Inset shows plots of the maximum Q-factors versus curvature ($r^{-1} = 2d^{-1}/\mu m^{-1}$). The broken line indicates the exploration of the least squares fit to the phenomenological equation; $Q = -574\ r^{-1}\ (\mu m^{-1}) + 663$.

We also coated the spheres with thin C_{60}-fullerene layers (thickness: 20 nm, Fig. S7f) and measured μ-PL. Because C_{60} acts as an electron acceptor for these polymers[1], we initially anticipated that the PL would be largely quenched via polymer-to-C_{60} electron transfer. However, clear WGM emissions were observed from the C_{60}-coated polymer spheres (Figs. S7a–S7d). The Q-factors were again dependent on d and reached as high as 540 (Fig. S7e). Because the estimated exciton diffusion length is in the range of 5–20 nm[1], the PL generated at the inner surface of the spheres accompanies the WGM peaks, even though the emission generated at the polymer/C_{60} interface would be largely quenched. Since the refractive index of C_{60} is larger than $\eta_{polymer}$ and in the range of 2.0–2.4[32], the confinement might be better for the C_{60}-coated polymer spheres.

Discussion

π-conjugated polymer microspheres act as fluorophores and resonators, as well as high-refractive-index media, and thus neither microfabrication nor dye doping are needed for the confinement and amplification of emission. The simple fabrication process via self-assembly of polymers easily affords micrometer-sized structures with very smooth surfaces and ideal topology, which is beneficial from the technological viewpoint. Because the fluorescence quantum yield of the present polymer spheres is not high[27], much better WGM photoemission properties are expected for spheres from polymers with higher fluorescence efficiency. Furthermore, by taking advantage of conducting polymers, electrically driven WGM emission might be possible, which would lead to the realization of novel polymer electroluminescence and lasing devices.

Methods

***μ*-PL measurements.** The samples were mounted in a micro-photoluminescence (μ-PL) measurement setup equipped with a long-distance 50× objective (NA = 0.5, Fig. S3)[22]. An optical microscope was used to identify suitable particles and to determine their diameters within an error margin of 0.2 μm. The spheres were excited on the circumference by a diode laser (Linos model Nano 250) with a 405 nm wavelength

with the power and spot size of 7 μW and ~0.5 μm, respectively. The photoluminescence was detected by a 0.5 m Czerny Turner spectrometer (Acton model SpectraPro 2500i, 0.26 nm resolution) with a LN_2-cooled charge-coupled device (CCD) detector.

Coating of the polymer spheres by TiO_x and C_{60}. A suspension of polymer microspheres was spin-cast onto 200-nm-thick SiO_2-covered Si substrate, and the substrates were set into a vacuum chamber (background pressure: $<1 \times 10^{-4}$ Pa). Ti or C_{60} were thermally evaporated at a deposition rate of 0.2 Å min^{-1}, forming a thin layer of Ti or C_{60} (thicknesses: 5 and 20 nm) at the large part of the surface of the spheres (Fig. S7f). Upon exposure to air, Ti was naturally oxidized to TiO_x.

1. Beaujuge, P. M. & Fréchet, J. M. J. Molecular design and ordering effects in π-functional materials for transistor and solar cell applications. *J. Am. Chem. Soc.* **133**, 20009–20029 (2011).
2. Kim, J. B. *et al.* Wrinkles and deep folds as photonic structures in photovoltaics. *Nature Photon.* **6**, 327–332 (2012).
3. Friend, R. H. *et al.* Electroluminescence in conjugated polymers. *Nature* **397**, 121–128 (1999).
4. Zaumseil, J., Friend, R. H. & Sirringhaus, H. Spatial control of the recombination zone in an ambipolar light-emitting organic transistor. *Nature Mater.* **5**, 69–74 (2006).
5. Muccini, M. A bright future for organic field-effect transistors. *Nature Mater.* **5**, 605–613 (2006).
6. Kozlov, V. G., Bulovi'c, V., Burrows, P. E. & Forrest, S. R. Laser action in organic semiconductor waveguide and double-heterostructure devices. *Nature* **389**, 362–364 (1997).
7. Samuel, I. D. W. & Turnbull, G. A. Organic semiconductor lasers. *Chem. Rev.* **107**, 1272–1295 (2007).
8. Uoyama, H., Goushi, K., Shizu, K., Nomura, H. & Adachi, C. Highly efficient organic light-emitting diodes from delayed fluorescence. *Nature* **492**, 234–240 (2012).
9. Vahala, K. J. Optical microcavities. *Nature* **424**, 839–846 (2003).
10. Matsko, A. B., Savchenkov, A. A., Strekalov, D., Ilchenko, V. S. & Maleki, L. Review of applications of whispering-gallery mode resonators in photonics and nonlinear optics. *IPN Prog. Rep.* **42–162**, 1–51 (2005).
11. Spillane, S. M., Kippenberg, T. J. & Vahara, K. J. Ultralow-threshold Raman laser using a spherical dielectric microcavity. *Nature* **415**, 621–623 (2002).
12. Armani, D. K., Kippenberg, T. J., Spillane, S. M. & Vahala, K. J. Ultra-high-*Q* toroid microcavity on a chip. *Nature* **421**, 925–928 (2003).
13. Finlayson, C. E. *et al.* Whispering gallery mode emission at telecommunications-window wavelengths using PbSe nanosrystals attached to photonic beads. *Semicond. Sci. Technol.* **21**, L21–L24 (2006).
14. Jiang, X.-F. *et al.* Highly unidirectional emission and ultralow-threshold lasing from on-chip ultrahigh-Q microcavities. *Adv. Mater.* **24**, OP260–OP264 (2012).
15. Frolov, S. V., Shkunov, M., Vardeny, Z. V. & Yoshino, K. Ring microlasers from conducting polymers. *Phys. Rev. B* **56**, R4363–R4366 (1997).
16. Kuwata-Gonokami, M. & Takeda, K. Polymer whispering gallery mode lasers. *Opt. Mater.* **9**, 12–17 (1998).
17. Liu, Z.-P. *et al.* Direct laser writing of whispering gallery microcavities by two-photon polymerization. *Appl. Phys. Lett.* **97**, 211105 (2010).
18. Ta, V. D., Chen, R. & Sun, H. D. Tuning whispering gallery mode lasing from self-assembled polymer droplets. *Sci. Rep.* **3**, 1362/1–5 (2013).
19. Ta, V. D., Chen, R., Ma, L., Ying, Y. J. & Sun, H. D. Whispering gallery mode microlasers and refractive index sensing based on single polymer fiber. *Laser Photon. Rev.* **7**, 133–139 (2013).
20. Tang, S. K. Y., Derda, R., Quan, Q., Loncar, M. & Whitesides, G. M. Continuously tunable microdroplet-laser in a microfluidic channel. *Opt. Exp.* **19**, 2204–2215 (2011).
21. Humar, M., Ravnik, M., Pajk, S. & Musevic, I. Electrically tubable liquid crystal optical microresonators. *Nature Photon.* **3**, 595–600 (2009).
22. Braam, D. *et al.* Role of the ligand layer for photoluminescence spectral diffusion of CdSe/ZnS nanoparticles. *Phys. Rev. B* **88**, 125302 (2013).
23. Pecher, J. & Mecking, S. Nanoparticles of conjugated polymers. *Chem. Rev.* **110**, 6260–6279 (2010).
24. Kuehne, A. J. C., Gather, M. C. & Sprakel, J. Monodisperse conjugated polymer particles by Suzuki-Miyaura dispersion polymerization. *Nature Commun.* **3**, 1088/1–7 (2012).
25. Anwar, N., Willms, T., Grimme, B. & Kuehne, A. J. C. Light-switchable and monodisperse conjugated polymer particles. *ACS Macro Lett.* **2**, 766–769 (2013).
26. Adachi, T. *et al.* Spherical assemblies from π-conjugated alternating copolymers: toward optoelectronic colloidal crystals. *J. Am. Chem. Soc.* **135**, 870–876 (2013).
27. Tong, L. *et al.* Tetramethylbithiophene in π-conjugated alternating copolymers as effective structural component for the formation of spherical assemblies. *Polym. Chem.* **5**, 3583–3587 (2014).
28. Kukino, M., Kuwabara, J., Matsuishi, K., Fukuda, T. & Kanbara, T. Synthesis and metal-like luster of novel polyaniline analogs containing azobenzene unit. *Chem. Lett.* **39**, 1248–1250 (2010).
29. Yamada, H. *et al.* Preparation and characterization of green reflective films of polyaniline analogs containing azobenzene units. *J. Appl. Polym. Sci. in press,* DOI:10.1002/app.41275.
30. Kuwata-Gonokami, M. *et al.* Polymer microdisk and microring lasers. *Opt. Lett.* **20**, 2093–2095 (1995).
31. Oraevsky, A. N. Whispering-gallery waves. *Quant. Elect.* **32**, 377–400 (2002).
32. Jensen, L. & van Duijnen, P. Th. Refractive index and third-order nonlinear susceptibility of C_{60} in the condensed phase calculated with the discrete solvent reaction field model. *Int. J. Quant. Chem.* **102**, 612–619 (2005).

Acknowledgments

This work was partly supported by a Grant-in-Aid for Young Scientists A (25708020) and Scientific Research on Innovative Areas (No. 25107507) from JSPS/MEXT, Japan, the Industrial Technology Research Grant Program (2011, NEDO, Japan), Cooperative Research Program of "Network Joint Research Center for Materials and Devices", Asahi Glass Foundation, Tokuyama Science Foundation, and University of Tsukuba-DAAD partnership program.

Author contributions

K.T., D.B. and A.B. carried out μ-PL and XSTEM experiments and analyzed the results. S.K. and L.T. prepared the polymer spheres and took SEM images. J.K. and T.K. synthesized the polymers. Y.Y. and A.L. designed the experiments, analyzed the data and wrote the manuscript.

Additional information

Reprints and permissions information is available online at http://npg.nature.com/reprintsandpermissions

Supplementary information accompanies this paper at http://www.nature.com/scientificreports

Competing financial interests: The authors declare no competing financial interests.

How to cite this article: Tabata, K. *et al.* Self-assembled conjugated polymer spheres as fluorescent microresonators. *Sci. Rep.* **4**, 5902; DOI:10.1038/srep05902 (2014).